Published in final edited form as:

Biochim Biophys Acta Mol Basis Dis. 2021 May 01; 1867(5): 166086. doi:10.1016/j.bbadis.2021.166086.

Deletion of Mcpip1 in Mcpip1$^{fl/fl}$Alb^{Cre} mice recapitulates the phenotype of human primary biliary cholangitis

Jerzy Kotlinowski[a,*], **Tomasz Hutsch**[b,c], **Izabela Czyzynska-Cichon**[d], **Marta Wadowska**[e], **Natalia Pydyn**[a], **Agnieszka Jasztal**[d], **Agnieszka Kij**[d], **Ewelina Dobosz**[e], **Maciej Lech**[e,f], **Katarzyna Miekus**[a], **Ewelina Pośpiech**[g], **Mingui Fu**[h], **Jolanta Jura**[a,1], **Joanna Koziel**[e,1], **Stefan Chlopicki**[d,i,1]

[a]Department of General Biochemistry, Faculty of Biochemistry, Biophysics and Biotechnology, Jagiellonian University, Gronostajowa 7, 30-387 Krakow, Poland

[b]Department of Experimental Physiology and Pathophysiology, Laboratory of Centre for Preclinical Research, Medical University of Warsaw, Pawińskiego 3c, 02-106 Warsaw, Poland

[c]Veterinary Diagnostic Laboratory ALAB bioscience, Stępińska 22/30, 00-739 Warszawa, Poland

[d]Jagiellonian Centre for Experimental Therapeutics (JCET), Jagiellonian University, Bobrzynskiego 14, 30-348 Krakow, Poland

[e]Department of Microbiology, Faculty of Biochemistry, Biophysics and Biotechnology, Jagiellonian University, Gronostajowa 7, 30-387 Krakow, Poland

[f]Department of Medicine IV, LMU Hospital, Munich, Germany

[g]Malopolska Centre of Biotechnology, Jagiellonian University, Kraków, Poland

[*]Corresponding author at: Gronostajowa Street 7, 30-387 Krakow, Poland. j.kotlinowski@uj.edu.pl (J. Kotlinowski).
[1]equal contribution as a senior author

CRedit authorship contribution statement

Jerzy Kotlinowski:Concept and design, Data acquisition, Analysis and interpretation of data, Writing and correcting the manuscript.
Tomasz Hutsch:Data acquisition, Analysis and interpretation of data.
Izabela Czyzynska-Cichon:Data acquisition.
Marta Wadowska:Data acquisition.
Natalia Pydyn:Data acquisition.
Agnieszka Jasztal:Data acquisition, Analysis and interpretation of data.
Agnieszka Kij:Data acquisition.
Ewelina Dobosz:Data acquisition.
Maciej Lech:Data acquisition.
Katarzyna Miekus:Data acquisition.
Ewelina Pośpiech:Analysis of RNA-seq data.
Mingui Fu:Providing Mcpip1$^{fl/fl}$ mice.
Jolanta Jura:Analysis and interpretation of data, Writing and correcting the manuscript.
Joanna Koziel:Concept and design, Analysis and interpretation of data, Writing and correcting the manuscript.
Stefan Chlopicki:Concept and design, Analysis and interpretation of data, Writing and correcting the manuscript

Declaration of competing interest

The authors declare that they have no known competing financial interests or personal relationships that could have appeared to influence the work reported in this paper.

Appendix A. Supplementary data

Supplementary data to this article can be found online at https://doi.org/10.1016/j.bbadis.2021.166086.

[h]Department of Biomedical Science and Shock/Trauma Research Center, School of Medicine, University of Missouri-Kansas City, Kansas City, USA

[i]Chair of Pharmacology, Jagiellonian University Medical College, Grzegorzecka 16, 31-531 Krakow, Poland

Abstract

Primary biliary cholangitis (PBC) is an autoimmune disease characterized by progressive destruction of the intrahepatic bile ducts. The immunopathology of PBC involves excessive inflammation; therefore, negative regulators of inflammatory response, such as Monocyte Chemoattractant Protein-1-Induced Protein-1 (MCPIP1) may play important roles in the development of PBC. The aim of this work was to verify whether Mcpip1 expression protects against development of PBC. Genetic deletion of *Zc3h12a* was used to characterize the role of Mcpip1 in the pathogenesis of PBC in 6–52-week-old mice. We found that Mcpip1 deficiency in the liver ($Mcpip1^{fl/fl}Alb^{Cre}$) recapitulates most of the features of human PBC, in contrast to mice with Mcpip1 deficiency in myeloid cells ($Mcpip1^{fl/fl}LysM^{Cre}$ mice), which present with robust myeloid cell-driven systemic inflammation. In $Mcpip1^{fl/fl}Alb^{Cre}$ livers, intrahepatic bile ducts displayed proliferative changes with inflammatory infiltration, bile duct destruction, and fibrosis leading to cholestasis. In plasma, increased concentrations of IgG, IgM, and AMA autoantibodies (anti-PDC-E2) were detected. Interestingly, the phenotype of $Mcpip1^{fl/fl}Alb^{Cre}$ mice was robust in 6-week-old, but milder in 12–24-week-old mice. Hepatic transcriptome analysis of 6-week-old and 24-week-old $Mcpip1^{fl/fl}Alb^{Cre}$ mice showed 812 and 8 differentially expressed genes, respectively, compared with age-matched control mice, and revealed a distinct set of genes compared to those previously associated with development of PBC. In conclusion, $Mcpip1^{fl/fl}Alb^{Cre}$ mice display early postnatal phenotype that recapitulates most of the features of human PBC.

Keywords

Primary biliary cholangitis; MCPIP1; Regnase1; Autoimmune disease; Inflammation

1. Introduction

Primary biliary cholangitis (PBC) is an autoimmune, chronic cholestatic liver disease, characterized by a slow, progressive destruction of the intrahepatic bile ducts. Features of the disease include inflammation leading to the destruction of small- and medium-sized intrahepatic bile ducts, development of fibrosis, and granulomas, and may lead to cirrhosis [1]. The prevalence of PBC ranges from 1.91 to 40.2 per 100,000 people, with the important, yet unexplained, hallmark of predominance in females [2,3]. Unfortunately, the factors leading to PBC are not fully understood. Environmental stimuli, as well as interacting immunogenetic and epigenetic risk factors, have been proposed contributors [4,5]. For example, pollution, tobacco smoke, toxin exposure, or infectious agents (e.g., *E. coli*) are considered promoters of PBC development [3,6,7]. Additionally, it has been shown by many studies that family history and genetic predisposition are important factors in PBC risk

and etiology. In monozygotic twins, the concordance rate is 63%, and for the first-degree relatives of PBC patients, concordance is 4% [3,6].

The main symptoms of PBC are not specific and include fatigue, skin hyperpigmentation, pruritus (itchy skin), hepatosplenomegaly, and xanthelasmas. Portal hypertension or jaundice may also occur in PBC. However, 20%–60% of PBC cases are diagnosed in asymptomatic patients based on the detection of antimitochondrial autoantibodies (AMA), which are associated with the elevation of IgM and cholestatic biochemistry, and then confirmed by the presence of specific bile duct pathology assessed via liver biopsy [6]. The presence of AMA, targeted to pyruvate dehydrogenase (PDC-E2), branched chain 2-oxo-acid dehydrogenase and 2-oxo-glutaric acid dehydrogenase is a highly specific marker that is identified in about 95% of patients with PBC [7].

Although it is clear that the pathophysiology of PBC is linked to an intense autoimmune response directed against biliary epithelial cells, the mechanism of biliary destruction remains enigmatic. The immunopathology of PBC is consistent with the dysregulation of both adaptive and innate immunity, resulting in excessive activity of various inflammatory cells [8]. Several specific mechanisms have been postulated, including IL-12-JAK-STAT4 signaling, Th1 T cell polarization, CD80 or IFN-gamma-dependent pathways, as well as the involvement of liver-infiltrating autoreactive T cells (CD4+ T cells, CD8+ T cells, natural killer T cells, and B cells) [1].

The activation of inflammatory cells is controlled on transcriptional and posttranscriptional levels by Monocyte Chemoattractant Protein-Induced Protein 1 (MCPIP1, *alias* Regnase1), which is involved in negative regulation of inflammation through its endonuclease activity [9,10] that shortens the half-life of selected pro-inflammatory cytokine transcripts (e.g., IL-1β, IL-6, IL-8) and mitigates their function [11–13]. The anti-inflammatory properties of MCPIP1 have been confirmed *in vivo* [9,14–16], but it is not known whether MCPIP1 controls the autoimmune response in patients with PBC. Recently, Sun et al. described a protective role of Mcpip1 in liver recovery after ischemia/reperfusion (I/R) injury, indicating that Mcpip1 functions to ameliorate liver damage, reduce inflammation, prevent cell death, and promote tissue regeneration, but authors did not study the role of MPCIP1 in the context of autoimmune liver disease [17].

To verify the hypothesis that Mcpip1 expression protects against the development of autoimmune liver disease, we generated mice lacking Mcpip1 in liver cells ($Mcpip1^{fl/fl}Alb^{Cre}$). Their phenotype recapitulated features of human biliary cholangitis as evidenced by increased levels of immunoglobulins (IgG, IgM) as well as AMA and anti-nuclear autoantibodies (ANA, anti-PDC-E2, anti-gp-210, respectively), liver fibrosis, inflammation, and destruction of intrahepatic bile ducts that led to cholestasis.

2. Materials and methods

2.1. Animals and genotyping

Animals were housed in ventilated cages under specific pathogen-free conditions in a temperature-controlled environment with a 14/10 h light/dark cycle and fed ad libitum

with standard laboratory chow food (Altromin). To obtain hepatocyte-specific knockout of the *Zc3h12a* gene encoding Mcpip1, *Zc3h12a*$^{lox/lox}$ mice (Mcpip1$^{fl/fl}$), with loxp sites flanking exon 3 of the *Zc3h12a* gene [16], were crossed with liver-specific Cre-expressing transgenic mice (Alb$^{Cre\ tg/+}$, Jackson Laboratory). The mice were designated as Mcpip1$^{fl/fl}$Alb^{Cre}. Deletion of Mcpip1 in leukocytes of myeloid origin was achieved after crossing Mcpip1$^{fl/fl}$ mice with a LysM-Cre expressing strain (LysM$^{Cre\ tg/+}$, Jackson Laboratory). The mice were designated Mcpip1$^{fl/fl}$LysM^{Cre}. For genotyping, DNA was extracted from tail tissue using the KAPA Mouse Genotyping Kit (KAPA Biosystems) according to the manufacturer's instructions. Genotyping for loxp insertion was performed by PCR using the following primers: GCCTTCCTGATCCTATTGGAG (wild-type), GAGATGGCGCAGCGCAATTAAT (knock-out), and GCCTCTTGTCACTCCCTCCTCC (common). Genotyping for Alb$^{Cre\ tg/+}$ was conducted with the following primers: TGCAAACATCACATGCACAC (wild-type), GAAGCAGAAGCTTAGGAAGATGG (mutant), and TTGGCCCCTTACCATAACTG (common), and genotyping for LysM^{Cre} was performed using TTACAGTCGGCCAGGCTGAC (wild-type), CCCAGAAATGCCAGATTACG (mutant), and CTTGGGCTGCCAGAATTTCTC (common). The Local Animal Ethical Commission approved all experiments.

2.2. Collection of tissue and organs

Blood and organs were always harvested between 9 a.m. and 12.00 a. m. Anesthesia with ketamine and xylazine was followed by blood collection from the orbital sinus. Next, livers and spleens were dissected, weighted and liver lobes were divided for RNA and protein isolation (lobus hepatis sinister medialis and sinister lateralis) and histology (lobus hepatis dexter medialis and dexter lateralis, lobus hepatis caudatus).

2.3. Histological evaluation of liver pathology in Mcpip1$^{fl/fl}$Alb^{Cre} mice

Liver samples obtained from male and female mice of different ages were fixed in 4% buffered formalin and processed through the standard paraffin embedding method. Sections of 5 μm were stained with hematoxylin and eosin (HE) for general histology and Picro Sirius Red (PSR) for collagen deposition, and then visualized using a standard light microscope (Olympus BX51; Olympus Corporation). Qualitative evaluation of liver samples was performed under 200× and 400× magnification. For quantitative analysis of fibrosis, PSR-stained sections were imaged under 100× magnification and the degree of collagen deposition was analyzed using the Ilastik segmentation toolkit and Fiji ImageJ software (NIH, Bethesda, MD, United States). The number of bile ducts was calculated from counts within 10 randomly chosen portal areas per liver section, under 200× magnification in a blinded fashion, using a standard light microscope (Olympus BX41; Olympus Corporation).

2.4. Immunohistochemical staining

5 μm paraffin sections were deparaffinated with standard protocol, followed by heat-mediated epitopes retrieval. For staining the EnVision G2 Doublestain System, Rabbit/Mouse (DAB+/Permanent Red) Kit (Dako) was used. The following anti-mouse primary antibodies were used: Cytokeratin 19 (Abcam), Cd3 (Bio-Rad), F4/80 (NovusBio), Ly6C (Serotec), B220 (Invitrogen). Next, liver samples were mounted with glycerol mounting medium (Dako), and examined with a Leica DMI6000 B microscope (Leica Microsystems).

For quantitative analysis, cells were counted in 10 high power fields from 5 mice in the group. Samples stained with anti-mouse Ck19 antibodies were additionally counterstained with Mayer's hematoxylin (Sigma).

2.5. Transcriptome sequencing

Prior to library preparation, RNA sample integrity was evaluated and concentration was measured using an Agilent 2100 Bioanalyzer with an RNA 6000 Pico Kit (Agilent). Libraries for 16 samples were prepared using the Ion AmpliSeq™ Transcriptome Mouse Gene Expression Kit, which covers over 20,000 mouse RefSeq genes in a single assay. Libraries were prepared according to the manufacturer's protocol using 50 ng of total RNA as input. Sixteen barcoded libraries were combined and pooled in equimolar concentrations and subsequently sequenced on two chips from the Ion PI Chip Kit v3 using an Ion Proton Sequencer and Ion PI Hi-Q Sequencing 200 chemistry. The primary bioinformatic analyses, including filtering and alignment of reads, were carried out using Torrent Suite Server v5.10.0. Subsequently, reads were counted and subjected to differential expression analysis using the DESeq2 package (with default parameters) implemented in R version 3.3.3. *P*-values for differentially expressed genes were corrected for multiple comparisons using the Benjamini-Hochberg approach and results with corrected *p*-values <0.05 were considered significant. Functional annotation of differentially expressed genes (≥ 1.2-fold change) was performed using bioinformatic tools available via the Database for Annotation, Visualization and Integrated Discovery (DAVID; version 6.8; https://david.ncifcrf.gov/home.jsp). Gene lists were searched using Ensembl gene annotation (ENSEMBL_GENE_ID), with the *Mus musculus* background dataset used for analyses. Selected genes were mapped to Biological Process (BP) Gene Ontology (GO) terms. Venn diagrams were created using the InteractiVenn tool [18]. Principal component analysis (PCA) was conducted for RNA-Seq data to demonstrate differential gene expression in the analyzed cell types. PCA analysis and subsequent plot generation were conducted using DESeq2 and ggplot2 libraries in R.

2.6. Statistical analysis

Results are expressed as mean ± SEM. The exact number of experiments or animals used is indicated in figure legends. Two-tailed Student's *t*-test was used for comparison of two groups, and one-way ANOVA with Bonferroni post hoc test was applied for comparison of multiple groups. Statistical significance is indicated by asterisks in figures, with the following definitions: * $p < 0.05$; ** $p < 0.01$; *** $p < 0.001$.

For further details regarding the materials and methods used, please refer to the supplementary information.

3. Results

3.1. Development of liver-specific Zc3h12a-deficient mice

To study the function of Mcpip1 protein in vivo, we generated $Mcpip1^{fl/fl}Alb^{Cre}$ knockout mice which lack the *Zc3h12a* gene in liver cells. As previously described by Li and colleagues [16], murine embryonic stem cells were genetically modified to obtain a loxp knock-in flanking the 3rd exon of the *Zc3h12a* gene. After generation of chimeric mice

and a series of backcrosses, the C57BL/6N *Zc3h12afl/fl* mice were obtained (Fig. S1A). Control Mcpip1$^{fl/fl}$ and Mcpip1$^{fl/fl}$Alb^{Cre} mice were selected after standard genotyping (Fig. S1B), and deletion of the *Zc3h12a* gene was confirmed in Mcpip1$^{fl/fl}$Alb^{Cre} mice at both the RNA and protein levels (Fig. S1C,D). The knockout mice showed diminished *Zc3h12a* expression in the liver and primary hepatocytes, but not in the heart and lungs, confirming liver specificity of Mcpip1 silencing (Fig. S1C,D).

3.2. General characteristics of Mcpip1$^{fl/fl}$Alb^{Cre} mice

Mcpip1$^{fl/fl}$Alb^{Cre} mice were born at the expected Mendelian ratio and had no gross abnormalities or impairment in general fitness (mobility, activity (lethargy), alopecia, presence of wounds and piloerection) up to 52 weeks of age compared to Mcpip$^{fl/fl}$ mice (data not shown). There were no differences in body mass of Mcpip1$^{fl/fl}$Alb^{Cre} versus control mice, however, Mcpip1$^{fl/fl}$Alb^{Cre} animals were characterized by hepatomegaly and splenomegaly (Fig. S1E–G). Blood morphology parameters of 6, 24, and 52-week-old Mcpip1$^{fl/fl}$Alb^{Cre} animals did not differ significantly from Mcpip1$^{fl/fl}$ counterparts (Table 1). Alkaline phosphatase (ALP) activity and concentration of total bile acids (TBA) in the serum of 6-week-old Mcpip1$^{fl/fl}$Alb^{Cre} mice were both significantly higher than in control animals (Table 2). In 52-week-old Mcpip1$^{fl/fl}$Alb^{Cre} mice, TBA was also higher compared with that of age-matched controls, but the difference did not reach significance ($p = 0.083$). In contrast to young and old Mcpip1$^{fl/fl}$Alb^{Cre} mice, 24-week-old Mcpip1$^{fl/fl}$Alb^{Cre} mice did not show any differences in biochemical parameters compared with their Mcpip1$^{fl/fl}$ counterparts (Table 2).

3.3. Histological and serological pathology of Mcpip1$^{fl/fl}$Alb^{Cre} mice recapitulates human primary biliary cholangitis

Mcpip1$^{fl/fl}$Alb^{Cre} mice at 6–52 weeks of age, but not Mcpip1$^{fl/fl}$ mice, displayed characteristic liver pathology, including active and progressive proliferation of intrahepatic bile ducts accompanied by extensive parenchymal inflammation and fibrosis, along with fibrosis in portal areas, all at various intensities depending on age (Fig. 1, S3–S5). Interestingly, first symptoms of PBC in Mcpip1$^{fl/fl}$Alb^{Cre} mice were already detected in 10-day-old pups (Fig. S2).

All features of intrahepatic bile duct pathology were extensive in 6-week-old Mcpip1$^{fl/fl}$Alb^{Cre} mice, however, at 24 weeks of age, histopathological changes were less severe in the liver parenchyma. By 52 weeks of age, the histopathological features of PBC were modestly reintensified in Mcpip1$^{fl/fl}$Alb^{Cre} mice (Fig. 1C,D,G,H).

In 6-week-old Mcpip1$^{fl/fl}$Alb^{Cre} mice, active and intensive collagen deposition was associated with extensive bile duct hyperplasia and inflammation (Fig. 1E, S4). At the ages of 12 and 24 weeks, proliferation and inflammatory processes diminished temporarily and the area of fibrotic tissue was reduced (Fig. 1F,G, S4). However, recurrence of intrahepatic and periportal cholangiocytes' proliferation with inflammatory infiltration in livers of 52-week-old animals led to reactivation of collagen deposition (Fig. 1H, S4). The entire spectrum of features of intrahepatic bile duct pathology was present in 52-week-old Mcpip1$^{fl/fl}$Alb^{Cre} mice, as shown in Fig. 2A–H. The extensive proliferation of bile ducts in

the liver parenchyma and portal areas was accompanied by bile duct epithelium disruption, inflammation, and fibrosis, resulting in lumen obstruction and bile duct destruction (Fig. 2A–C). Eventually, the closure of intrahepatic bile duct lumen, bile acid deposition in hepatocytes, and formation of small granulomas were observed (Fig. 2D–F).

To further assess the similarities between the phenotype of Mcpip1$^{fl/fl}$Alb^{Cre} mice and the characteristics of PBC in humans, levels of total IgG, IgM, and specific AMA and ANA were measured. IgG and IgM concentrations were higher in 6 and 24-week-old Mcpip1$^{fl/fl}$Alb^{Cre} animals compared to Mcpip1$^{fl/fl}$ counterparts (Fig. 2I,J). Additionally, 60–90% of Mcpip1$^{fl/fl}$Alb^{Cre} mice had higher plasma concentrations of anti-PDC-E2 mitochondrial autoantibodies than control counterparts (Fig. 2K). Incidence of anti-gp-210 nuclear autoantibodies, was elevated in 12-week-old Mcpip1$^{fl/fl}$Alb^{Cre} mice and reached 90% (Fig. 2L).

Mcpip1$^{fl/fl}$Alb^{Cre} mice of all ages showed increased leukocytes infiltration into the liver parenchyma in comparison to Mcpip1$^{fl/fl}$ controls (Fig. 3A–C). Lymphocytes T were predominant population of leukocytes infiltration in 6-week-old mice, while 24-week-old Mcpip1$^{fl/fl}$Alb^{Cre} animals were characterized by additional accumulation of lymphocytes B, macrophages and neutrophils. Finally, only in 6-week-old Mcpip1$^{fl/fl}$Alb^{Cre} mice expression of cholangiocytes' marker – cytokeratin 19 (Ck19) – was significantly increased (Fig. 3D–F).

To verify whether systemic inflammation caused by lack of Mcpip1 protein in myeloid cells might also lead to PBC development, Mcpip1$^{fl/fl}$LysM^{Cre} mice were analyzed. Features of human PBC were not observed in Mcpip1$^{fl/fl}$LysM^{Cre} mice, despite the presence of robust myeloid cell-driven systemic inflammation (Fig. S6).

3.4. Male and female Mcpip1$^{fl/fl}$Alb^{Cre} mice have the same pathological features

In humans, PBC is disease with high predominance in females. We therefore compared the phenotype of female and male Mcpip1$^{fl/fl}$Alb^{Cre} mice. Histological comparison of liver sections from 6, 12, and 24-week-old Mcpip1$^{fl/fl}$Alb^{Cre} mice revealed no differences in the development of pathology between female and male mice. All characteristic features of intrahepatic bile duct pathology demonstrated in male Mcpip1$^{fl/fl}$Alb^{Cre} mice were also present in female Mcpip1$^{fl/fl}$Alb^{Cre} mice, including a similar pattern of collagen deposition in the liver (Fig. S7A). There was also no difference between male and female Mcpip1$^{fl/fl}$Alb^{Cre} mice in plasma levels of anti-PDC-E2 and anti-gp-210 autoantibodies (Fig. S7B).

3.5. Transcriptome changes in Mcpip1-depleted primary hepatocytes

To better understand the molecular mechanisms responsible for the robust PBC phenotype in 6-week-old Mcpip1$^{fl/fl}$Alb^{Cre} mice and its downregulation in 24-week-old Mcpip1$^{fl/fl}$Alb^{Cre} mice, the transcriptome of isolated primary hepatocytes was analyzed. Differential gene expression analysis followed by calculation of *p*-values revealed that, in 6 and 24-week-old Mcpip1$^{fl/fl}$Alb^{Cre} mice, there were 812 and 8 differentially expressed genes (DEGs), respectively, compared with their respective age-matched controls.

In hepatocytes derived from 6-week-old Mcpip1$^{fl/fl}$Alb^{Cre} mice, 688 DEGs were upregulated and 124 were downregulated (Table S1 in the Supplementary Material). As shown in Fig. 4, upregulated genes were related to cell cycle control (e.g., cell division, mitotic nuclear division, cell cycle, positive regulation of cell proliferation), regulation of inflammation (e.g., inflammatory response, immune response, cytokine-mediated signaling, IL-1β and IL-6 production), and extracellular matrix biosynthesis (e.g., extracellular matrix and collagen fibril organization, collagen biosynthesis, extracellular matrix constituent secretion). Downregulated genes were related to lipid metabolism (e.g., lipid metabolic processes, fatty acid (FA) β-oxidation, FA and cholesterol metabolic processes, FA transport, negative regulation of lipid storage), oxidation-reduction processes, glucose homeostasis, and organic anion transport (Fig. 4).

In hepatocytes from 24-week-old Mcpip1$^{fl/fl}$Alb^{Cre} mice, only 8 genes were differently expressed compared to age-matched control mice (upregulated in Mcpip1$^{fl/fl}$Alb^{Cre}: *Lpin1, Lrp6*, and *Tmc7*; downregulated in Mcpip1$^{fl/fl}$Alb^{Cre}: *Cela1, Ppdpf, Asap1, Lect2*, and *Pla2g16*; Table S2 in the Supplementary Material).

The striking difference between the transcriptomes of 6 and 24-week-old Mcpip1$^{fl/fl}$Alb^{Cre} versus their respective controls was also confirmed by direct comparison of the transcriptomes of hepatocytes from 6 and 24-week-old Mcpip1$^{fl/fl}$Alb^{Cre} mice, which showed 725 DEGs, with 538 upregulated and 187 downregulated (Fig. S8, Table S3 in the Supplementary Material). This comparison revealed similar enhanced processes (mitotic nuclear division, cell cycle, and cell division) when hepatocytes isolated from 6-week-old control and knockout mice were compared.

4. Discussion

We have, to our knowledge, been the first to demonstrate that the phenotype of Mcpip1$^{fl/fl}$Alb^{Cre} mice recapitulates most features of human PBC (Table 3). On a histopathological level, Mcpip1$^{fl/fl}$Alb^{Cre} mice displayed intrahepatic bile duct pathology that included active proliferative changes, inflammatory infiltration, bile duct epithelium disruption, small granuloma formation, and significant and progressive liver fibrosis in the parenchyma and portal areas. On a functional level, Mcpip1$^{fl/fl}$Alb^{Cre} mice showed cholestasis. Autoimmune response, a characteristic feature of PBC, was also detected in Mcpip1$^{fl/fl}$Alb^{Cre} mice, as demonstrated by increased plasma concentrations of IgG and IgM, as well as AMA and ANA autoantibodies (anti-PDC-E2, anti-gp-210). As Mcpip1 deficiency in myeloid cells (Mcpip1$^{fl/fl}$LysM^{Cre} mice) did not result in features of PBC, we concluded that Mcpip1, specifically in the liver, is a negative regulator of autoimmune response and may protect against PBC development. Importantly, our results showed that Mcpip1$^{fl/fl}$Alb^{Cre} mice had robust postnatal symptomatology, displayed a mild phenotype in middle age, and seem to regain PBC features in older age. Transcriptomic analysis of primary hepatocytes revealed a distinct set of genes compared to those previously linked to PBC, and identified distinct transcriptomes for early and chronic phases of PBC. Altogether, Mcpip1$^{fl/fl}$Alb^{Cre} mice represent a unique model that closely mimics PBC in humans (see Table 3 for summary) and has significant potential to increase insight into the pathophysiology of PBC.

Previously described murine models of PBC, including genetically modified models, xenobiotic immunized models, and infection-triggered models display some important features of PBC, such as the presence of AMA, elevated levels of IgG and IgM, portal lymphocyte infiltration, and bile duct destruction [19]. However, they do not recapitulate all features of PBC; for example, other mouse models do not display progressive fibrosis, a central clinical feature that informs prognosis, including morbidity and mortality, in human PBC patients [19]. Although Mcpip1$^{fl/fl}$Alb^{Cre} mice do not show female predominance of PBC features, which has been observed in only one PBC model (IFNγ-ARE-Del mice) [20], the Mcpip1$^{fl/fl}$Alb^{Cre} mouse model has the advantage of clinical relevance via its unambiguous histopathological features and full spectrum of PBC-associated pathological changes that are not comprehensively present in any previously described model (Figs. 1, 2, S4, S5). Importantly, fibrosis was present in 100% of Mcpip1$^{fl/fl}$Alb^{Cre} mice, compared to approximately 50% of IL-12p35−/−;dnTGFβRII double mutant mice [21]. Another unique feature of Mcpip1$^{fl/fl}$Alb^{Cre} mice is the robust postnatal PBC phenotype followed by remission in middle age, that is not driven by systemic inflammation, but by intrinsic liver-derived pathology. Although it is not known whether PBC in humans has MCPIP1-driven pathogenesis, peak incidence of PBC in humans occurs in the fifth decade of life; timing that seems compatible with the mild phenotype in middle-aged Mcpip1$^{fl/fl}$Alb^{Cre} mice. Mcpip1$^{fl/fl}$Alb^{Cre} mice are prone to PBC development, however it does not progress to fully-blown complications in 52-week-old mice. Lack of Mcpip1 in liver cells triggers this disease acting as a ‘first-hit’ that must be apparently followed by a ‘second-hit’ for the development of PBC into fully-blown phenotype in older mice. This seem in line with the number of known factors that precipitate PBC in humans [4,5,22]. In this regard, it would be tempting to test if Mcpip1$^{fl/fl}$Alb^{Cre} mice subjected to known PBC risk factors (toxins, chemicals, inflammatory factors), will respond with accelerated disease progression after exposure.

The Mcpip1$^{fl/fl}$Alb^{Cre} mouse model of PBC presented here differs from other models on both the phenotype and genomic levels. Previously, PBC mouse model development was driven by alteration of function of various genes, including *Ifng* [20], *Tgfbr2* [23], *Il2ra* (IL-2Rα−/−) [24], *Foxp3* [25], *Il12a* [21] and *Slc4a2* [26], yet none of these genes was found to be differentially expressed in hepatocytes isolated from Mcpip1$^{fl/fl}$Alb^{Cre} mice. Indeed, Mcpip1$^{fl/fl}$Alb^{Cre} mice displayed a unique set of DEGs in hepatocytes, with a strikingly distinct profile of DEGs in early and chronic phases of the disease in 6 and 24-week-old Mcpip1$^{fl/fl}$Alb^{Cre} mice, respectively.

In 6-week-old Mcpip1$^{fl/fl}$Alb^{Cre} mice with early phase PBC, we identified enhanced expression of many genes involved in cell proliferation (e.g., *Hgf, Tgfb1, Wnt2*), as well as genes involved in biliary development and cholangiocyte proliferation and important for biliary repair (e.g., *Hgf, Pdgfa, Tgfb1, Bmp2, Mmp9*), fibrosis (e.g., *Tgfb1, Lpin1*), inflammation (e.g., *Il1a, Il1b, ccl2, Cxcl2, Cxcl12, S100a8, S100a9*), or extracellular matrix organization (e.g., *Mmp9, Col1a1, Col3a1*).

In contrast to early phase PBC with 812 DEGs, the chronic remission phase showed only 8 DEGs, including altered expression of *Lrp6*, *Lect2*, and *Lipin-1*. Low-density lipoprotein receptor-related protein 6 (Lrp6) linked with the Wnt/β-catenin signaling

pathway was shown to regulate liver fibrosis [27]. Leukocyte cell-derived chemotaxin-2 (*LECT2*), originally identified as a hepatocyte-secreted chemokine [28] was identified as a prognostic indicator in acute liver failure [29,30]. Finally, *Lipin-1* (*Lpin1*), the only gene with significantly different expression in knockout cells at both time points, was shown to coactivate HNF4α and regulate fatty acid catabolism [31] and TGF-β-induced fibrogenesis [32].

Mcpip1$^{fl/fl}$Alb^{Cre} mice also showed altered expression of organic anion transporters encoding Organic anion transporting polypeptide 1a1 (Oatp1a1 protein, *Slco1a1* gene) and Organic anion transporter 2 (Oat2 protein, *Slc22a7* gene), which are involved in bile acid transport [33]. These changes are likely primary to the PBC phenotype in Mcpip1$^{fl/fl}$Alb^{Cre} mice and compatible with the changes in expression of other organic transporters, such as NTCP, OATP1B1, and OATP1B3 in humans with PBC [34].

Although the expression of multiple genes were altered by the deletion of Mcpip1 alone, it seems impossible to identify a single signaling pathway responsible for the observed PBC phenotype in Mcpip1$^{fl/fl}$Alb^{Cre} mice, and changes in expression of multiple genes and their interactions are likely responsible. Although some genes differently expressed in the remission phase could be linked to liver fibrosis and liver failure, their roles in this PBC phenotype remain to be established, along with links between the early and chronic phases of PBC and the mechanisms of activation of the disease phenotype in aging Mcpip1$^{fl/fl}$Alb^{Cre} mice.

Finally, although Mcpip1$^{fl/fl}$Alb^{Cre} mice develop PBC, the molecular mechanism leading to this phenotype have not been defined here and needs to be elucidated. Interestingly, Alb-Cre construct was shown to drive gene deletion not only in hepatocytes, but also in cholangiocytes, activated stellate cells and hepatoblasts [35]. Hepatoblasts are progenitor cells, that differentiate into both hepatocytes and cholangiocytes during liver development [36]. Murine liver starts to develop at embryonic day 8.5 and between E13.5-E16.5 hepatoblasts begin to differentiate into mature cells – hepatocytes and cholangiocytes [37]. Albumin expression in hepatoblasts starts around embryonic day 13.5, which means that by using Alb-Cre construct, deletion of gene should be achieved not only in hepatocytes, but also in cholangiocytes [36,37]. In line with this data, we detected depletion of Mcpip1 protein both in hepatocytes and cholangiocytes isolated from Mcpip1$^{fl/fl}$Alb^{Cre} mice (unpublished observations). Thus, the future studies should verify, whether lack of Mcpip1 protein in Mcpip1$^{fl/fl}$Alb^{Cre} mice is linked to a hepatocyte-driven or cholangocyte-driven mechanism leading to cholangiocytes' pathology and PBC development. Establishment of molecular link between Mcpip1 and PBC would be possible, for example by testing phenotype of mice with deletion of Mcpip1 only in cholangiocytes but not in hepatocytes.

Nevertheless, our work has demonstrated the novel role of Mcpip1 as a protein orchestrating biliary duct hemostasis and identified that the PBC phenotype results from Mcpip1 deficiency in the liver. Thus far, MCPIP1 is primarily known for its anti-inflammatory properties that are mediated via endonuclease activity and result in shortening the half-life of selected pro-inflammatory cytokine transcripts (e.g., IL-1β, IL-6, IL-8) and mitigating their function [9,10,13,38]. In a number of reports, the role of Mcpip1 in immune response

has been demonstrated in vivo [9,27,39,40] and some reports suggested the involvement of Mcpip1 in autoimmune response; for example, in autoimmune gastritis and lupus [41]. Our study extends the knowledge of Mcpip1 as a regulator of autoimmune response in the liver, as we demonstrated that Mcpip1 deficiency triggered autoimmunity against bile ducts and led to the PBC phenotype.

In conclusion, our study demonstrated that Mcpip1 expression in the liver is a key protective factor against development of PBC. Mcpip1$^{fl/fl}$Alb^{Cre} mice represent an excellent model to investigate the molecular mechanisms responsible for PBC development and to test novel treatment strategies for PBC.

Supplementary Material

Refer to Web version on PubMed Central for supplementary material.

Financial support statement

This work was supported by research grants from National Science Centre, Poland nos. 2015/19/D/NZ5/00254 and 2017/27/B/NZ5/01440 to JeKo, and 2018/29/B/NZ6/01622 to JoKo. The open-access publication of this article was funded by the Priority Research Area BioS under the program “Excellence Initiative - Research University” at the Jagiellonian University in Krakow.

Abbreviations:

ALP	alkaline phosphatase
AMA	antimitochondrial autoantibodies
ANA	anti-nuclear autoantibodies
BSA	bovine serum albumin
DEG	differentially expressed gene
FA	fatty acid
HE	hematoxylin and eosin
I/R	ischemia/reperfusion
LC-MS	liquid chromatography-mass spectrometry
LSEC	liver sinusoidal endothelial cells
PBC	primary biliary cholangitis
PBS	phosphate-buffered saline
PCA	principal component analysis
TBA	total bile acid

References

[1]. Webb GJ, Siminovitch KA, Hirschfield GM, The immunogenetics of primary biliary cirrhosis: a comprehensive review, J Autoimmun [Internet]. 64 (2015 Nov 1) 42–52 [Cited 2020 Mar 25]; Available from, http://www.ncbi.nlm.nih.gov/pubmed/26250073. [PubMed: 26250073]

[2]. Boonstra K, Beuers U, Ponsioen CY. Epidemiology of primary sclerosing cholangitis and primary biliary cirrhosis: a systematic review, J Hepatol [Internet]. 56 (5) (2012 May) 1181–1188 [cited 2020 Mar 26]; Available from, http://www.ncbi.nlm.nih.gov/pubmed/22245904. [PubMed: 22245904]

[3]. Purohit T, Cappell MS. Primary biliary cirrhosis: Pathophysiology, clinical presentation and therapy. World J Hepatol [Internet]., [Cited 2020 Mar 26];7(7): 926–41, Available from, http://www.ncbi.nlm.nih.gov/pubmed/25954476, 2015 May 8. [PubMed: 25954476]

[4]. Juran BD, Lazaridis KN, Environmental factors in primary biliary cirrhosis, Semin. Liver Dis. 34 (3) (2014) 265–272.

[5]. Bianchi I, Carbone M, Lleo A, Invernizzi P, Genetics and epigenetics of primary biliary cirrhosis, Semin Liver Dis [Internet]. 34 (3) (2014 Aug) 255–264 [cited 2020 Mar 26]; Available from, http://www.ncbi.nlm.nih.gov/pubmed/25057949. [PubMed: 25057949]

[6]. Lleo A, Marzorati S, Anaya J-M, Gershwin ME, Primary biliary cholangitis: a comprehensive overview, Hepatol Int [Internet]. 11 (6) (2017 Nov 1) 485–499 [cited 2020 Mar 26]; Available from, http://www.ncbi.nlm.nih.gov/pubmed/29164395. [PubMed: 29164395]

[7]. Carey EJ, Ali AH, Lindor KD, Primary biliary cirrhosis, in: The Lancet Vol. 386, Lancet Publishing Group, 2015, pp. 1565–1575.

[8]. Ma WT, Chen DK, Immunological abnormalities in patients with primary biliary cholangitis [Internet], in: Clinical Science Vol. 133, Portland Press Ltd, 2019 [cited 2020 Mar 25]. p. 741–60. Available from, http://www.ncbi.nlm.nih.gov/pubmed/30890652. [PubMed: 30890652]

[9]. Matsushita K, Takeuchi O, Standley DM, Kumagai Y, Kawagoe T, Miyake T, et al. , Zc3h12a is an RNase essential for controlling immune responses by regulating mRNA decay, Nature [Internet]. 458 (7242) (2009 Apr 30) 1185–1190 [cited 2020 Mar 25]; Available from, http://www.ncbi.nlm.nih.gov/pubmed/19322177. [PubMed: 19322177]

[10]. Mizgalska D, Wegrzyn P, Murzyn K, Kasza A, Koj A, Jura J, et al. , Interleukin-1-inducible MCPIP protein has structural and functional properties of RNase and participates in degradation of IL-1beta mRNA, FEBS J [Internet]. 276 (24) (2009) 7386–7399. Dec [cited 2018 Jul 19]; Available from: http://doi.wiley.com/10.1111/j.1742-4658.2009.07452.x. [PubMed: 19909337]

[11]. Mino T, Murakawa Y, Fukao A, Vandenbon A, Wessels H-H, Ori D, et al. , Regnase-1 and roquin regulate a common element in inflammatory mRNAs by spatiotemporally distinct mechanisms, Cell [Internet]. 161 (5) (2015 May 21) 1058–1073 [cited 2020 Mar 26]; Available from: http://www.ncbi.nlm.nih.gov/pubmed/26000482. [PubMed: 26000482]

[12]. Lipert B, Wilamowski M, Gorecki A, Jura J, MCPIP1, alias Regnase-1 binds and cleaves mRNA of C/EBPβ, in: Kim YK (Ed.), PLoS One [Internet] vol. 22, 2017 Mar [cited 2018 Jul 19];12(3):e0174381. Available from: 10.1371/journal.pone.0174381. [PubMed: 28328949]

[13]. Dobosz E, Wilamowski M, Lech M, Bugara B, Jura J, Potempa J, et al. , MCPIP1, alias regnase-1, controls epithelial inflammation by posttranscriptional regulation of IL-8 production, J Innate Immun [Internet]. 8 (6) (2016 Nov 1) 564–578 [cited 2020 Mar 26]; Available from: http://www.ncbi.nlm.nih.gov/pubmed/27513529. [PubMed: 27513529]

[14]. Liang J, Saad Y, Lei T, Wang J, Qi D, Yang Q, et al. , MCP-induced protein 1 deubiquitinates TRAF proteins and negatively regulates JNK and NF-kappaB signaling, J Exp Med [Internet]. 207 (13) (2010 Dec) 2959–2973, 20 [cited 2018 Jul 19]; Available from: http://www.jem.org/lookup/doi/10.1084/jem.20092641. [PubMed: 21115689]

[15]. Uehata T, Iwasaki H, Vandenbon A, Matsushita K, Hernandez-Cuellar E, Kuniyoshi K, et al. , Malt1-induced cleavage of regnase-1 in CD4(+) helper T cells regulates immune activation, Cell [Internet]. 153 (5) (2013 May 23) 1036–1049, cited 2020 Mar 25]; Available from: http://www.ncbi.nlm.nih.gov/pubmed/23706741. [PubMed: 23706741]

[16]. Li Y, Huang X, Huang S, He H, Lei T, Saaoud F, et al. , Central role of myeloid MCPIP1 in protecting against LPS-induced inflammation and lung injury, Signal Transduct Target Ther

[Internet]. 8 (2017 Dec) [cited 2018 Jul 19];2:17066. Available from: http://www.nature.com/articles/sigtrans201766. [PubMed: 29263935]

[17]. Sun P, Lu YX, Cheng D, Zhang K, Zheng J, Liu Y, et al. , Monocyte chemoattractant protein-induced protein 1 targets hypoxia-inducible factor 1α to protect against hepatic ischemia/reperfusion injury, Hepatology [Internet]. 1 (2018 Dec) [cited 2020 Jul 9];68(6):2359–75. Available from: https://pubmed.ncbi.nlm.nih.gov/29742804/. [PubMed: 29742804]

[18]. Heberle H, Meirelles GV, da Silva FR, Telles GP, Minghim R, InteractiVenn: a web-based tool for the analysis of sets through Venn diagrams, BMC Bioinformatics [Internet]. 16 (1) (2015 May 22) 169 [cited 2020 Mar 25];16(1):169. Available from: http://www.ncbi.nlm.nih.gov/pubmed/25994840. [PubMed: 25994840]

[19]. Katsumi T, Tomita K, Leung PSC, Yang G-X, Gershwin ME, Ueno Y, Animal models of primary biliary cirrhosis, Clin Rev Allergy Immunol [Internet]. 48 (2–3) (2015 Jun 1) 142–153 [cited 2020 Mar 25]; Available from: http://www.ncbi.nlm.nih.gov/pubmed/25771770. [PubMed: 25771770]

[20]. Bae HR, Leung PSC, Tsuneyama K, Valencia JC, Hodge DL, Kim S, et al. , Chronic expression of interferon-gamma leads to murine autoimmune cholangitis with a female predominance, Hepatology [Internet]. 64 (4) (2016 Oct 1) 1189–1201 [cited 2020 Mar 25]; Available from: http://www.ncbi.nlm.nih.gov/pubmed/27178326. [PubMed: 27178326]

[21]. Tsuda M, Zhang W, Yang G-X, Tsuneyama K, Ando Y, Kawata K, et al. , Deletion of interleukin (IL)-12p35 induces liver fibrosis in dominant-negative TGFβ receptor type II mice, Hepatology [Internet]. 57 (2) (2013 Feb) 806–816 [cited 2020 Mar 25]; Available from: http://www.ncbi.nlm.nih.gov/pubmed/22576253. [PubMed: 22576253]

[22]. Lleo A, Marzorati S, Anaya JM, Gershwin ME, Primary biliary cholangitis: a comprehensive overview [Internet], in: Hepatology International Vol. 11, Springer, 2017, pp. 485–499 [cited 2020 Jul 9]. Available from: https://pubmed.ncbi.nlm.nih.gov/29164395/. [PubMed: 29164395]

[23]. Oertelt S, Lian Z-X, Cheng C-M, Chuang Y-H, Padgett KA, He X-S, et al. , Anti-mitochondrial antibodies and primary biliary cirrhosis in TGF-β receptor II dominant-negative mice, J Immunol [Internet]. 177 (3) (2006 Aug 1) 1655–1660 [cited 2020 Mar 25];177(3):1655–60. Available from: http://www.ncbi.nlm.nih.gov/pubmed/16849474. [PubMed: 16849474]

[24]. Wakabayashi K, Lian ZX, Moritoki Y, Lan RY, Tsuneyama K, Chuang YH, et al. , IL-2 receptor α−/− mice and the development of primary biliary cirrhosis, Hepatology [Internet]. 44 (5) (2006 Nov) 1240–1249 [cited 2020 Mar 25]; Available from: http://www.ncbi.nlm.nih.gov/pubmed/17058261. [PubMed: 17058261]

[25]. Zhang W, Sharma R, Ju S-T, He X-S, Tao Y, Tsuneyama K, et al. , Deficiency in regulatory T cells results in development of antimitochondrial antibodies and autoimmune cholangitis, Hepatology [Internet]. 49 (2) (2009 Feb) 545–552 [cited 2020 Mar 25]; Available from: http://www.ncbi.nlm.nih.gov/pubmed/19065675. [PubMed: 19065675]

[26]. Salas JT, Banales JM, Sarvide S, Recalde S, Ferrer A, Uriarte I, et al. , Ae2a,b-deficient mice develop antimitochondrial antibodies and other features resembling primary biliary cirrhosis, Gastroenterology [Internet]. 134 (5) (2008 May) 1482–1493 [cited 2020 Mar 25]; Available from: http://www.ncbi.nlm.nih.gov/pubmed/18471521. [PubMed: 18471521]

[27]. Yu F, Du F, Wang Y, Huang S, Miao R, Major AS, et al. , Bone marrow deficiency of MCPIP1 results in severe multi-organ inflammation but diminishes atherogenesis in hyperlipidemic mice, PLoS One [Internet]. 8 (11) (2013 Nov 6), e80089 [cited 2020 Mar 26]; Available from: http://www.ncbi.nlm.nih.gov/pubmed/24223214. [PubMed: 24223214]

[28]. Lebensztejn DM, Flisiak-Jackiewicz M, Białokoz-Kalinowska I, Bobrus-Chociej A, Kowalska I, Hepatokines and non-alcoholic fatty liver disease, Acta Biochim Pol [Internet]. 63 (3) (2016) 459–467 [cited 2020 Jul 9]; Available from: https://pubmed.ncbi.nlm.nih.gov/27262842/. [PubMed: 27262842]

[29]. Sato Y, Watanabe H, Kameyama H, Kobayashi T, Yamamoto S, Takeishi T, et al. , Serum LECT2 level as a prognostic indicator in acute liver failure, in: In: Transplantation Proceedings [Internet]. Transplant Proc, 2004 [cited 2020 Jul 9]. p. 2359–61. Available from: https://pubmed.ncbi.nlm.nih.gov/15561249/. [PubMed: 15561249]

[30]. Slowik V, Borude P, Jaeschke H, Woolbright BL, Lee WM, Apte U, Leukocyte cell derived chemotaxin-2 (Lect2) as a predictor of survival in adult acute liver failure, Transl

Gastroenterol Hepatol [Internet]. 1 (2019 Mar) [cited 2020 Jul 9];4 (March). Available from: https://pubmed.ncbi.nlm.nih.gov/30976720/. [PubMed: 30854488]

[31]. Chen Z, Gropler MC, Mitra MS, Finck BN, Complex interplay between the lipin 1 and the hepatocyte nuclear factor 4 α (HNF4α) pathways to regulate liver lipid metabolism, PLoS One [Internet]. 7 (2012 Dec) [cited 2020 Jul 9];7(12). Available from: https://pubmed.ncbi.nlm.nih.gov/23236470/.

[32]. Jang CH, Kim KM, Yang JH, Cho SS, Kim SJ, Shin SM, Cho SHK IJ, The role of lipin-1 in the regulation of fibrogenesis and TGF-β signaling in hepatic stellate cells - PubMed [Internet], Toxicol Sci. (2016) 28–38 [cited 2020 Jul 9]. p. 28–38. Available from: https://pubmed.ncbi.nlm.nih.gov/27345520/. [PubMed: 27345520]

[33]. Roth M, Obaidat A, Hagenbuch B, OATPs, OATs and OCTs: the organic anion and cation transporters of the SLCO and SLC22A gene superfamilies, British Journal of Pharmacology 165 (2012) 1260–1287. [PubMed: 22013971]

[34]. Thakkar N, Slizgi JR, Brouwer KLR, Effect of liver disease on hepatic transporter expression and function, J Pharm Sci [Internet]. 106 (9) (2017 Sep 1) 2282–2294 [cited 2020 Mar 25]; Available from: http://www.ncbi.nlm.nih.gov/pubmed/28465155. [PubMed: 28465155]

[35]. Lemaigre FP, Determining the fate of hepatic cells by lineage tracing: facts and pitfalls, Hepatology [Internet]. 61 (6) (2015 Jun 1) 2100–2103 [cited 2020 Mar 25]; Available from: http://www.ncbi.nlm.nih.gov/pubmed/25503476. [PubMed: 25503476]

[36]. Miyajima A, Tanaka M, Itoh T, Stem/progenitor cells in liver development, homeostasis, regeneration, and reprogramming, Cell Stem Cell [Internet]. 14 (5) (2014 May 1) 561–574 [cited 2020 Mar 26]; Available from: http://www.ncbi.nlm.nih.gov/pubmed/24792114. [PubMed: 24792114]

[37]. Tanaka M, Okabe M, Suzuki K, Kamiya Y, Tsukahara Y, Saito S, et al. , Mouse hepatoblasts at distinct developmental stages are characterized by expression of EpCAM and DLK1: drastic change of EpCAM expression during liver development, Mech Dev [Internet]. 126 (8–9) (2009 Aug) 665–676 [cited 2020 Mar 26]; Available from: http://www.ncbi.nlm.nih.gov/pubmed/19527784. [PubMed: 19527784]

[38]. Mino T, Murakawa Y, Fukao A, Vandenbon A, Wessels H-H, Ori D, et al. , Regnase-1 and roquin regulate a common element in inflammatory mRNAs by spatiotemporally distinct mechanisms, Cell [Internet]. 21 (2015 May) [cited 2018 Jul 19];161(5):1058–73. Available from: http://linkinghub.elsevier.com/retrieve/pii/S0092867415004468. [PubMed: 26000482]

[39]. Liang J, Saad Y, Lei T, Wang J, Qi D, Yang Q, et al. , MCP-induced protein 1 deubiquitinates TRAF proteins and negatively regulates JNK and NF-kappaB signaling, J Exp Med [Internet]. 207 (2010 Dec 20) 2959–2973 [cited 2020 Mar 25]; Available from: http://www.ncbi.nlm.nih.gov/pubmed/21115689. [PubMed: 21115689]

[40]. Peng H, Ning H, Wang Q, Lu W, Chang Y, Wang TT, et al. , Monocyte chemotactic protein-induced protein 1 controls allergic airway inflammation by suppressing IL-5-producing TH2 cells through the Notch/Gata3 pathway, J Allergy Clin Immunol [Internet]. 142 (2) (2018 Aug 1) 582–594.e10 [cited 2020 Mar 25]; Available from: http://www.ncbi.nlm.nih.gov/pubmed/29111212. [PubMed: 29111212]

[41]. Zhou Z, Miao R, Huang S, Elder B, Quinn T, Papasian CJ, et al. , MCPIP1 deficiency in mice results in severe anemia related to autoimmune mechanisms, PLoS One [Internet]. 8 (12) (2013 Dec 6), e82542 [cited 2020 Mar 25]; Available from: http://www.ncbi.nlm.nih.gov/pubmed/24324805. [PubMed: 24324805]

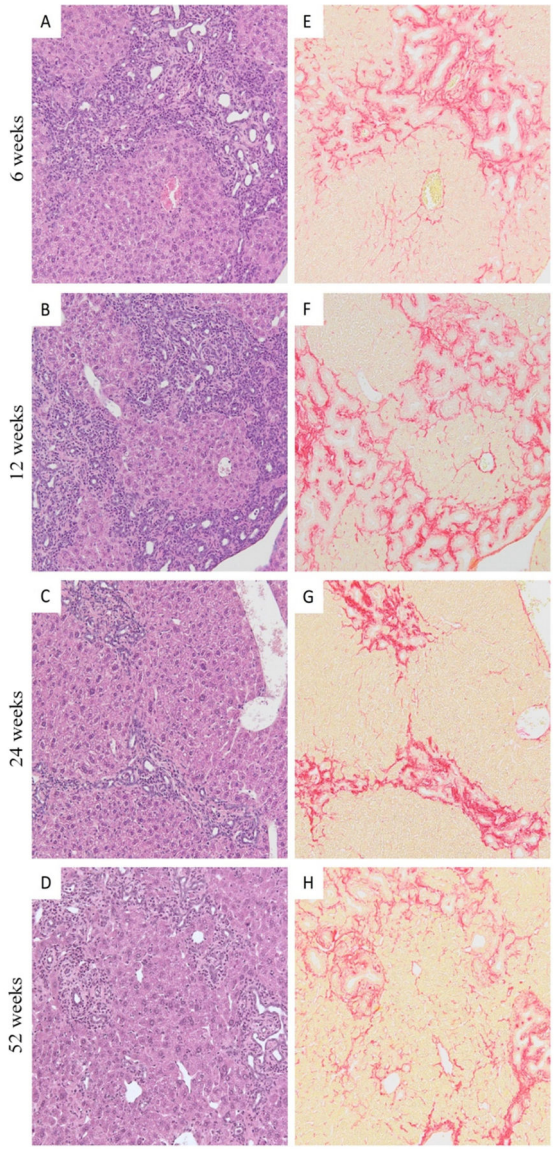

Fig. 1.

Progression of intrahepatic bile duct pathology in the liver parenchyma of 6 to 52-week-old Mcpip1$^{fl/fl}$Alb^{Cre} male mice.

Proliferative changes in intrahepatic bile ducts with inflammatory infiltration predominate in young (6-week-old) mice leading to bile duct destruction, intraductal obstruction, and extensive fibrosis. At the age of 24 weeks, the processes of proliferation, inflammation, and collagen deposition were reduced, while aged mice (52-week-old) developed new foci of cholangiocyte proliferation accompanied by active fibrotic areas. Magnification 200×, HE (A-D) and PSR (*E*-H) staining. HE, hematoxylin and eosin; PSR, picrosirius red. For Mcpip1$^{fl/fl}$ $n = 5$ and for Mcpip1$^{fl/fl}$Alb^{Cre} $n = 10$.

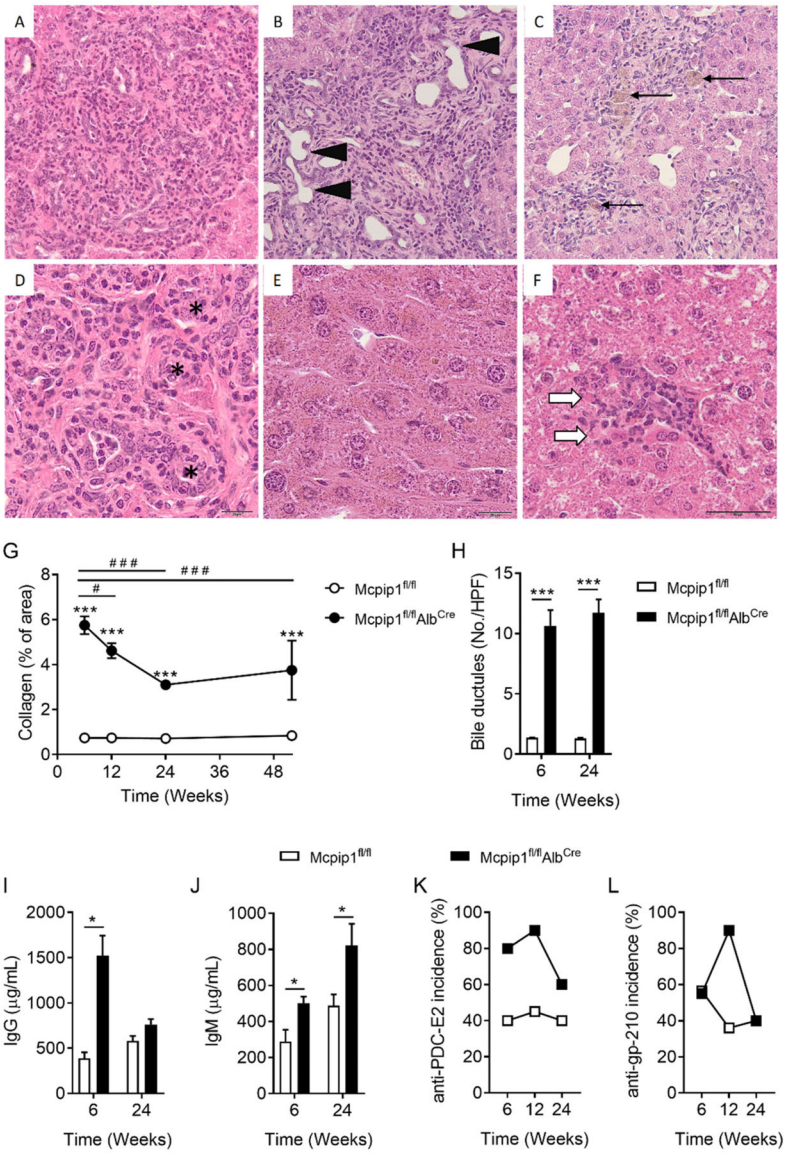

Fig. 2.

Characterization of hallmarks of primary biliary cholangitis in Mcpip1$^{fl/fl}$Alb^{Cre} mice. HE staining of 52-week-old mice showing (A) Proliferation of intrahepatic bile ducts with associated parenchymal inflammation; (B) Epithelial destruction of intrahepatic bile ducts (black arrows) and extensive fibrosis of parenchyma; (C) Resolution of inflammation in intrahepatic bile ducts involving macrophages (black arrows); (D) Dysplasia of cholangiocytes with associated intraductal obstruction of intrahepatic bile ducts (asterisks); (E) Cholestasis and bile acid deposition in hepatocytes; (F) Small granuloma (white arrows indicate hepatocyte necrosis), magnification 400×. (G) Collagen area in the liver of 6, 12, 24, and 52-week-old Mcpip1$^{fl/fl}$ and Mcpip1$^{fl/fl}$Alb^{Cre} mice; (H) Number of bile ductules in livers per high power field (HPF); Concentrations of total IgG (I) and IgM (J) classes in plasma of 6 and 24-week-old Mcpip1$^{fl/fl}$ and Mcpip1$^{fl/fl}$Alb^{Cre} mice; Percentage of mice, with higher concentration of anti-PDC-E2 antimitochondrial autoantibodies (K) and anti-

gp-210 antinuclear autoantibodies (L) compared to mean concentration in control Mcpip1$^{fl/fl}$ counterparts. For Mcpip1$^{fl/fl}$ $n = 5$ (Fig. 2), for Mcpip1$^{fl/fl}$Alb^{Cre} $n = 10$ (Fig. 2A–G, I–L) and n = 5 (Fig. 2H). Data represent mean ± SEM, *$p < 0.05$, ***$p < 0.001$ vs. Mcpip1$^{fl/fl}$; #$p < 0.05$, ##$p < 0.01$; ###$p < 0.001$ vs. 6 weeks. HE, hematoxylin and eosin.

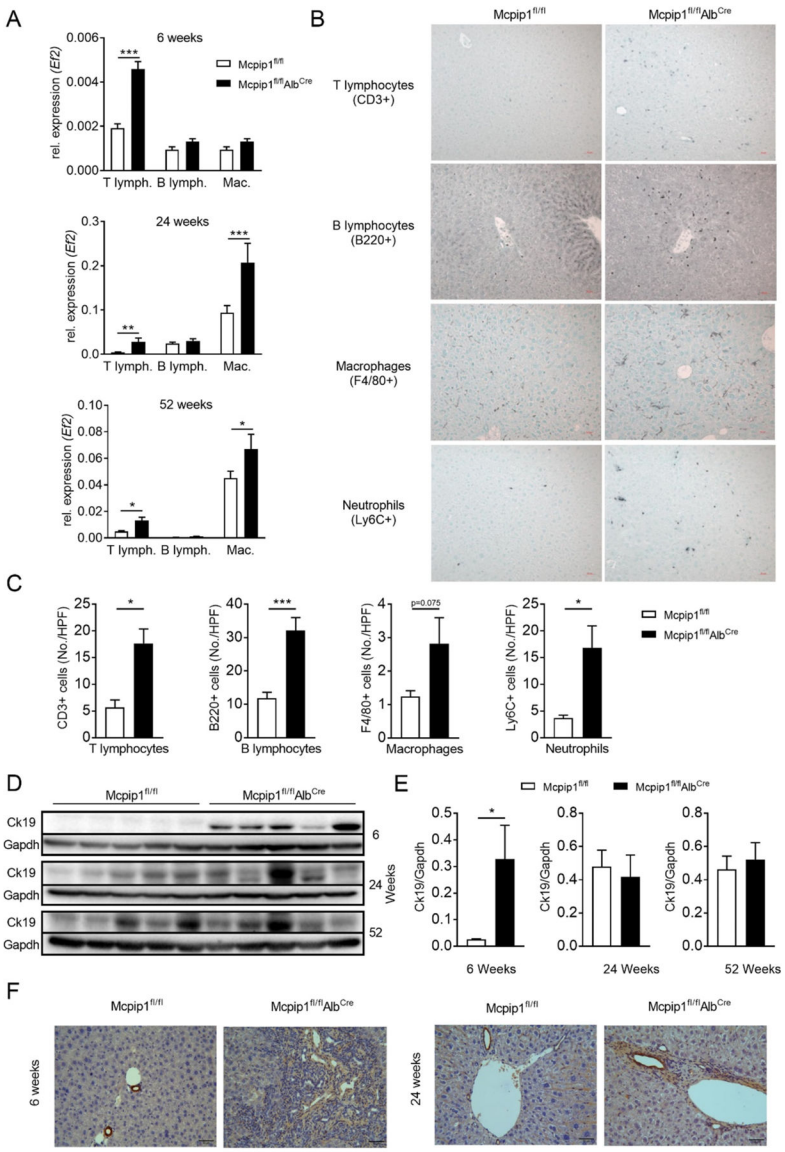

Fig. 3.

Characterization of lymphocytic infiltration into livers of Mcpip1$^{fl/fl}$Alb^{Cre} mice. (A) Real-time PCR analysis of specific leukocytes markers: expression of *Cd3e* (T lymphocytes), *Cd19* (B lymphocytes) and *Adgre1* (macrophages) in livers of 6, 24 and 52-week-old Mcpip1$^{fl/fl}$ and Mcpip1$^{fl/fl}$Alb^{Cre} mice; (B) representative immunohistological stainings and (C) quantitative analysis of leukocytes classes detected in 24-week-old control and Mcpip1$^{fl/fl}$Alb^{Cre} animals; (D) western blot analysis and (E) densitometric analysis of cytokeratin 19 (Ck19) protein level in 6, 24 and 52-week-old mice; (F) representative immunohistological stainings of Ck19 in 6 and 24-week-old control and Mcpip1$^{fl/fl}$Alb^{Cre} animals. For Mcpip1$^{fl/fl}$ and for Mcpip1$^{fl/fl}$Alb^{Cre} $n = 5$. Data represent mean ± SEM, *$p <$ 0.05, ***$p < 0.001$ vs. Mcpip1$^{fl/fl}$.

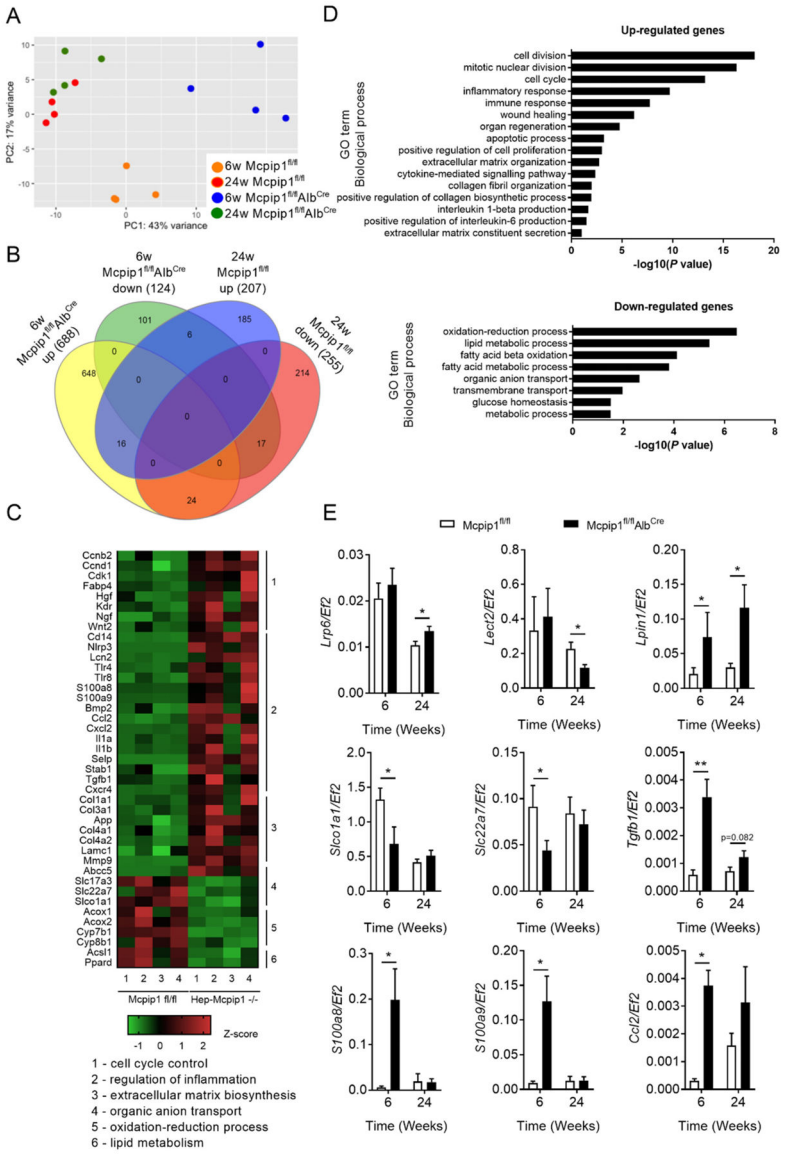

Fig. 4.

Transcriptome analysis of Mcpip1$^{fl/fl}$ and Mcpip1$^{fl/fl}$Alb^{Cre} primary hepatocytes. (A) PCA plot for RNA-Seq dataset demonstrating differential gene expression in all analyzed primary hepatocytes isolated from 6 and 24-week-old Mcpip1$^{fl/fl}$ (6w Mcpip1$^{fl/fl}$, 24w Mcpip1$^{fl/fl}$, respectively) and 6 and 24-week-old Mcpip1$^{fl/fl}$Alb^{Cre} mice (6w Mcpip1$^{fl/fl}$Alb^{Cre}, 24w Mcpip1$^{fl/fl}$Alb^{Cre}, respectively); (B) Venn diagram presenting the number of transcripts significantly up- and downregulated (adj. *P*-value <0.05) in 6-week-old Mcpip1$^{fl/fl}$Alb^{Cre} samples (6w Mcpip1$^{fl/fl}$Alb^{Cre} up/down) and 24-week-old Mcpip1$^{fl/fl}$ (24w Mcpip1$^{fl/fl}$ up/down) in comparison to 6-week-old Mcpip1$^{fl/fl}$ controls (6w Mcpip1$^{fl/fl}$); (C) Heat map showing differentially expressed genes selected from GO enrichment analysis; (D) GO enrichment analysis of genes differentially expressed in 6-week-old Mcpip1$^{fl/fl}$ and Mcpip1$^{fl/fl}$Alb^{Cre} primary hepatocytes. Scale is the −log10(P-value) of the enrichment score (*p*-value <0.05); (E) real-time PCR analysis of genes selected

after NGS analysis. For Mcpip1$^{fl/fl}$ and Mcpip1$^{fl/fl}$Alb^{Cre} $n = 4$ (Fig. 4A–D) and $n = 5$ (Fig. 4E). Data represent mean ± SEM, *$p < 0.05$, **$p < 0.01$ vs. Mcpip1$^{fl/fl}$.

Table 1

Blood counts of Mcpip1$^{fl/fl}$ and Mcpip1$^{fl/fl}$Alb^{Cre} mice.

Component	6 weeks		24 weeks		52 weeks	
	Mcpip1$^{fl/fl}$	**Mcpip1$^{fl/fl}$Alb^{Cre}**	**Mcpip1$^{fl/fl}$**	**Mcpip1$^{fl/fl}$Alb^{Cre}**	**Mcpip1$^{fl/fl}$**	**Mcpip1$^{fl/fl}$Alb^{Cre}**
Erythrocytes (*10^{12}/L)	9.19 ± 0.62	8.98 ± 0.83	9.73 ± 0.85	9.28 ± 0.61	10.45 ± 0.23	9.76 ± 0.26
Hemoglobin (g/dL)	15.03 ± 0.63	14.83 ± 0.98	14.52 ± 1.10	14.13 ± 0.93	14.75 ± 0.32	14.14 ± 0.31
Hematocrit (%)	46.19 ± 2.64	45.68 ± 4.28	45.67 ± 4.76	44.01 ± 2.57	51.17 ± 1.29	48.70 ± 1.17
MCV(fl)	50.43 ± 1.27	51.00 ± 0.82	46.83 ± 1.47	47.89 ± 1.17	49.17 ± 0.70	49.78 ± 0.57
MCH (pg)	16.39 ± 0.48	16.60 ± 0.42	14.93 ± 0.42	15.28 ± 0.19	14.12 ± 0.21	14.50 ± 0.20
MCHC (g/dL)	32.59 ± 0.81	32.53 ± 1.07	31.85 ± 0.87	31.89 ± 0.51	28.82 ± 0.27	29.03 ± 0.19
Platelets (*10^{9}/L)	749.0 ± 125.8	672.8 ± 80.1	989.3 ± 192.2	1051.3 ± 248.1	1314.6 ± 91.8	1342.3 ± 192.4
Leukocytes (*10^{9}/L)	3.74 ± 0.53	5.17 ± 0.56	5.97 ± 0.66	6.46 ± 0.65	5.65 ± 0.31	6.64 ± 0.82
Lymphocytes (*10^{9}/L)	2.09 ± 0.30	3.33 ± 0.29	3.90 ± 0.86	3.87 ± 1.16	3.88 ± 0.34	4.84 ± 1.07
Granulocytes (*10^{9}/L)	1.51 ± 0.20	1.48 ± 0.28	2.53 ± 0.56	2.37 ± 0.38	1.83 ± 0.11	2.74 ± 1.48
Monocytes (*10^{9}/L)	0.14 ± 0.04	0.28 ± 0.03	0.25 ± 0.04	0.31 ± 0.08	0.30 ± 0.04	0.40 ± 0.24

Data are presented as mean ± SEM, for Mcpip1$^{fl/fl}$ $n = 5$ and for Mcpip1$^{fl/fl}$Alb^{Cre} $n = 8$.

Biochim Biophys Acta Mol Basis Dis. Author manuscript; available in PMC 2022 May 01.

Table 2

Blood biochemistry of Mcpip1$^{fl/fl}$ and Mcpip1$^{fl/fl}$Alb^{Cre} mice.

Component	6 weeks		24 weeks		52 weeks	
	Mcpip1$^{fl/fl}$	**Mcpip1$^{fl/fl}$Alb^{Cre}**	**Mcpip1$^{fl/fl}$**	**Mcpip1$^{fl/fl}$Alb^{Cre}**	**Mcpip1$^{fl/fl}$**	**Mcpip1$^{fl/fl}$Alb^{Cre}**
ALT (U/L)	46.60 ± 6.91	50.36 ± 2.57	53.64 ± 8.28	48.39 ± 7.59	38.14 ± 6.37	92.40 ± 33.58
Albumin (g/dL)	3.33 ± 0.07	3.36 ± 0.05	3.15 ± 0.11	3.19 ± 0.09	3.64 ± 0.07	3.46 ± 0.13
AST (U/L)	125.9 ± 15.7	119.5 ± 12.6	141.8 ± 17.4	152.5 ± 10.8	116.5 ± 16.6	180.3 ± 46.9
Bilirubin (mg/dL)	0.06 ± 0.01	0.05 ± 0.01	0.10 ± 0.03	0.08 ± 0.01	Not detected	Not detected
Cholesterol (mg/dL)	99.11 ± 6.74	111.10 ± 3.01	95.14 ± 7.15	105.40 ± 5.73	93.25 ± 8.52	92.00 ± 9.63
ALP (U/L)	149.0 ± 12.0	287.7 ± 43.2 **	72.4 ± 1.8	75.1 ± 4.5	83.1 ± 4.6	108.3 ± 21.8
TBA (μmol/L)	7.3 ± 3.1	111.7 ± 28.2 **	Not analyzed	Not analyzed	40.9 ± 23.6	90.1 ± 21.6 $p = 0.083$

Data are presented mean ± SEM, for Mcpip1$^{fl/fl}$ $n = 5$ and for Mcpip1$^{fl/fl}$Alb^{Cre} $n = 8$.

Biochim Biophys Acta Mol Basis Dis. Author manuscript; available in PMC 2022 May 01.

Table 3

Comparison between characteristics of human PBC and Mcpip1$^{fl/fl}$Alb^{Cre}

Feature	Human PBC	Mcpip1$^{fl/fl}$Alb^{Cre}
Classification	Complex etiology	Genetic
Gender differences	Female predominance	No
Environmental factor	Yes	No
Elevated serum bile acids	Yes	Yes
Presence of autoantibodies:		
AMA	90–95%	60–90%
ANA	40–50%	40–90%
Immunoglobulins	IgM+; IgG+	IgM+; IgG+
Liver histology:		
Lymphocytic infiltration	Yes	Yes
Bile duct destruction	Yes	Yes
Granuloma	Yes	Yes
Fibrosis	Yes	Yes
Other findings		PBC phenotype was robust in 6-week-old mice, diminished in 24-week-old mice and modestly reintensified in 52-week-old mice